A Controllable Bidirectional Battery Charger for Electric Vehicles with Vehicle-to-Grid Capability

Hugo Neves de Melo, João Pedro F. Trovão, *Senior Member, IEEE*, Paulo G. Pereirinha, *Senior Member, IEEE*, Humberto M. Jorge, *Member, IEEE*, and Carlos Henggeler Antunes

***Abstract*—This paper proposes a comprehensive methodology for the design of a controllable electric vehicle charger capable of making the most of the interaction with an autonomous smart energy management system (EMS) in a residential setting. Autonomous EMSs aim achieving the potential benefits associated with energy exchanges between consumers and the grid, using bidirectional and power-controllable electric vehicle chargers. A suitable design for a controllable charger is presented, including the sizing of passive elements and controllers. This charger has been implemented using an experimental setup with a digital signal processor to validate its operation. The experimental results obtained foresee an adequate interaction between the proposed charger and a compatible autonomous EMS in a typical residential setting.**

***Index Terms*—Autonomous energy management system, plug-in electric vehicle, energy storage, bidirectional charger, grid-to-vehicle, vehicle-to-grid.**

I. Introduction

THE promotion of end-use energy efficiency policies as well as the deployment of technological solutions to materialize them represent a fundamental step contributing for sustainable development, which should be also associated with a higher penetration of renewable energy in the generation mix. The ongoing evolution of the present grids into smart grids, endowed with information and communication technologies (ICT), provides the technological basis for the development of more sustainable, intelligent and optimized energy management systems (EMS), such as the Energy Box (EB) previously proposed in [1], [2]. The EB exploits the usual flexibility that consumers have in load operation scheduling to obtain desired demand response actions and achieve optimal global control of energy resources (grid, loads, local generation and storage, including electric vehicles). EB inputs are price signals received from the grid in a dynamic tariff setting (usually depending on generation availability and grid status), user comfort requirements and constraints, weather conditions, local generation forecasts, etc., which will be used by algorithms to generate optimized control strategies. These strategies are beneficial to end-users, by lowering their electricity bill without degrading the quality of the energy services provided, and utilities/system operator, by assisting network management in face of a significant penetration of intermittent renewable generation [3], [4]. The EB can also display adaptive features, capture and learn the user's energy consumption profile and habitual behavior for more advanced energy management decisions predictability [1].

In this context, the implementation of this type of EMS faces some technological challenges such as the one addressed in this paper: the design of interface systems (controllable bidirectional chargers) between the grid and stationary and vehicular energy storage. The plug-in electric vehicle (PEV), i.e., a vehicle (all-electric or hybrid) that can be recharged through an electric plug (grid to vehicle, G2V), can be seen as a special residential load with the potential ability to return energy to the grid (vehicle to grid, V2G). Indeed, recent developments in PEV and residential EMS recognize the control of PEV charging and discharging operations as relevant issues on the way to sustainable mobility and global optimization of energy use [4].

The EB is responsible for controlling G2V/V2G operation modes through command signals acting as references to the charger controllers, as presented in [5], [6]. Together with load management, and possibly photovoltaic and wind micro-generation, the control of G2V/V2G operation modes has the capability to convert a residence or a neighborhood into a smart and potential stand-alone micro-grid.

This paper presents a methodology for the design and implementation of a bidirectional PEV charger, with adaptive capability in face of the available power information driven by demand

Manuscript received March 13, 2017; revised October 17, 2017; accepted November 10, 2017. Date of publication November 16, 2017; date of current version January 15, 2018. This work was supported by the Canada Research Chairs Program, the European Regional Development Fund through the COMPETE 2020 Program and the Portuguese FCT within project SAICTPAC/0004/2015-POCI-01-0145-FEDER-016434, Suspense project CENTRO-01-0145-FEDER-000006, and FCT under Project Grant UID/MULTI/00308/2013. The review of this paper was coordinated by the Guest Editors of the VPPC 2016 Special Section. *(Corresponding author: João Pedro F. Trovão.)*

H. Neves de Melo was with the Institute for Systems and Computers Engineering at Coimbra, 3030-290 Coimbra, Portugal. He is now with Energias de Portugal, 1249-300 Lisbon, Portugal (e-mail: hugomigueldemelo@gmail.com).

J. P. F. Trovão was with the Department of Electrical Engineering, Polytechnic Institute of Coimbra-Coimbra Institute of Engineering, 3030-199 Coimbra, Portugal. He is now with the Department of Electrical Engineering and Computer Engineering, Université de Sherbrooke, Sherbrooke, QC, J1K 2R1, Canada, and also with the Institute for Systems and Computers Engineering at Coimbra, 3030-290 Coimbra, Portugal (e-mail: Joao.Trovao@USherbrooke.ca).

P. G. Pereirinha is with the Department of Electrical Engineering, Coimbra Institute of Engineering, Polytechnic Institute of Coimbra, 3030-199 Coimbra, Portugal, and also with the Institute for Systems and Computers Engineering at Coimbra, 3030-290 Coimbra, Portugal (e-mail: ppereiri@isec.pt).

H. M. Jorge and C. H. Antunes are with the Department of Electrical and Computer Engineering, University of Coimbra, 3030-290 Coimbra, Portugal, and also with the Institute for Systems and Computers Engineering at Coimbra, 3030-290 Coimbra, Portugal (e-mail: hjorge@deec.uc.pt; ch@deec.uc.pt).

Color versions of one or more of the figures in this paper are available online at http://ieeexplore.ieee.org.

Digital Object Identifier 10.1109/TVT.2017.2774189

coming from an autonomous EMS, through the exchange of monitoring and control signals.

A simulation model of the system has been developed allowing to obtain estimates for monthly electricity expenses regarding the use of the PEV in real data scenarios [6], [7]. In [8], an infrastructure for dynamic power control of battery chargers is proposed, adjusting the battery current in charging mode. In [9], a bidirectional battery charger with V2G and vehicle to home (V2H) capability is proposed, which also deals with active and reactive power control. In [10] reference charger currents are set for each PEV managed by an aggregator performing the allocation of active and reactive individual EV set-points. The bidirectional structure proposed in [11] also displays active and reactive control capabilities in G2V and V2G operation modes, complemented with a modular charge equalizer circuit to improve the battery performance by means of an integrated control strategy. The design and control of a bidirectional battery charger for EVs, and its operation as an active power filter when connected to the local home electrical grid is described in [12]. The charger is also designed and controlled to operate during the charging of the battery from the grid and the injection of the power back to the grid when needed. A single-phase reconfigurable battery charger operating in G2V, V2G and traction-to-auxiliary (T2A) modes, in which the auxiliary battery is charged from the traction batteries, is proposed in [13]. The main operation modes of present and prospective battery chargers in smart grids and smart homes are discussed in [14]. In addition to G2V and V2G, this paper proposes a home-to-vehicle (H2V) operation mode, in which the current of the EV battery charger depends on the consumption of electrical appliances. Moreover, in the vehicle-for-grid (V4G) mode the PEV battery charger is used to compensate current harmonics or reactive power.

The simplicity of the proposed architecture and the control layer (for G2V and V2G), the adaptability to the residential voltage levels and EMS set-points, and the adequate values of THD (Total Harmonic Distortion) are key elements of recent research reported in literature.

This paper focuses on the design and testing of a PEV battery charger, which allows for PEV charging or discharging given the available power and other information dynamically provided by an EMS, instead of minimizing the charging time by using only the maximum power level. A simple and functional power electronics topology has been used to validate the concept. The design of the charger was based on reference works such as the ones mentioned in [15], [16]. Other topologies, which may be categorized as isolated or non-isolated, are discussed in [17], [18], to address some improvement gains and efficiency. For instance, the usage of the three-phase motor winding to DC or AC operation is proposed in [15]. Furthermore, charge is not confined to DC, since most chargers have direct plug to AC due to the space that EVs are now taking in the automotive market [19].

Despite more complicated topologies are available in the literature, the proposed approach can fulfill the desired principles of operation for the bidirectional charger in the operational framework of an EMS. For this purpose, the sizing of some passive elements and the design of power electronics converters controllers have been developed to maintain the current and voltage levels within the bounds, fulfilling power quality (PQ) requirements. The main features of the proposed approach are: 1) compatibility with EMS, such as the EB, autonomously optimizing energy resources in a residential setting; 2) active and reactive control in G2V and V2G operation with THD in accordance with international standards; 3) concern with battery-life time, displaying smooth power variation in charge and discharge modes; 4) control strategy of the charge equalizer circuit is fully integrated into the charger control algorithm; 5) modular structure to increase reliability and flexibility.

The proposed structure and control scheme have been validated with a small-scale prototype. The performance of the system has been evaluated in different operational conditions. Experimental results are quite promising, foreseeing an adequate interaction between the proposed charger and any compatible autonomous residential EMS.

In Section I, the interest, motivation and main contributions of this work are presented. Section II focuses on the power electronics charger topology and its analysis. Section III describes the design of the controllers. The experimental results obtained and their discussion are presented in Section IV. The main conclusions are drawn in Section V.

II. Power Electronics Charger Topology

PEV and their chargers are expected to become an increasingly relevant element of the grid. Since these chargers are the elements responsible for allowing establishing an optimized interface between the PEV and the grid, chargers and their associated intelligent management systems are key factors for PEV to become more competitive compared with Internal Combustion Engine (ICE) vehicles. Common topologies use non-controlled rectifiers, inverters, filters and DC/DC converters. Research has also been carried out regarding the control of active power, reactive power [10], [11] and voltage in this type of power converters [14], as referred to in Section I. Concerning the topology architectures, our proposal displays some similarities with the ones in [12] and [20], as well as with the approach of the controller in [11]. Regarding the developments stated in [11], [12] and [20], the proposal in this paper further demonstrates a proper and stable operation through a reduced-scale experimental setup. In this respect, the selection of power switches, controllers, filters, and the corresponding PQ impact revealed to be critical, as well as the mechanical assembly of all components to complete the final product [16].

A. Plug-in Electric Vehicle Charger Topology

The desirable characteristics for the charger are power bidirectionality (V2G and G2V), power factor equal to one, capability of performing power control, low PQ impact, construction and topology simplicity, and regular 16 A single-phase plug compatibility [6]. This charger does not allow performing fast charge, being 2.3 kW (10 A, 230 V) the advisable maximum power for a single-phase household-type plug [5], [21]. This power range is defined based on EU standards and power grid restrictions, since higher power ranges could represent a neg-

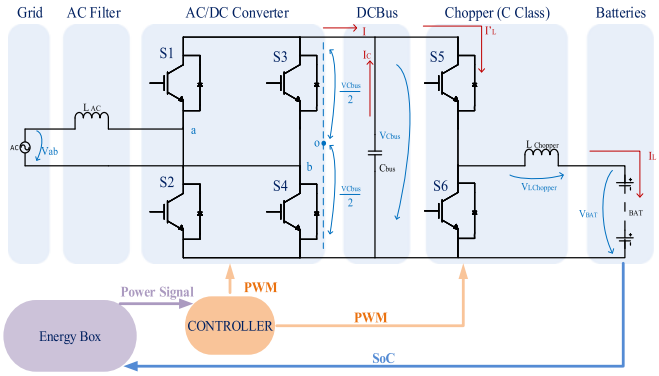

Fig. 1. PEV charger topology.

ative impact on the low voltage (LV) grid in terms of PQ and EMS requirements [22]–[24]. Regarding the voltage level of the battery pack, the proposed design is focused on L-category vehicles (two-, three- and four-wheel vehicles such as motorcycles, mopeds, quads, and minicars), as the one studied in [25], but could be extended to other voltage levels.

The topology presented in Fig. 1 is formed by three legs of two Insulated Gate Bipolar Transistors (IGBT), denoted by $S_j \in \{1, \ldots, 6\}$. The IGBTs are used due to their good compromise characteristics associated with voltage, switching frequency and current limits. These power switches are used for an AC/DC converter that operates as a controlled rectifier or as an inverter for G2V or V2G operation modes, respectively, and for a DC/DC converter (C class chopper) in which the power used for both modes is restricted, as discussed below. The features of converters meet the desired bi-directionality, where the chopper operates as buck and boost for G2V and V2G operation modes, respectively. Some passive elements for filtering and energy storage purposes are also designed and implemented, which are relevant for achieving proper system dynamics, stability and power quality.

B. DC/DC Converter Circuit Analysis

The DC/DC converter is a C class chopper, which allows operating in the first two quadrants (i.e., positive voltage and positive and negative current). The main operation equations can be synthetized through (1) to (4) and (5) to (8) for buck and boost operation modes, respectively.

$$V_{BAT} = V_{Cbus} - L_{Chopper} \cdot \frac{dI_L}{dt} \tag{1}$$

$$I_L = \frac{1}{L_{Chopper}} \cdot \int_0^{Ton} (V_{Cbus} - V_{BAT})\, dt \tag{2}$$

$$V_{BAT} = -L_{Chopper} \cdot \frac{dI_L}{dt} \tag{3}$$

$$I_L = \int_{Ton}^{Toff} -\frac{V_{BAT}}{L_{Chopper}} dt \tag{4}$$

$$V_{BAT} = L_{Chopper} \cdot \frac{dI_L}{dt} \tag{5}$$

$$I_L = \frac{1}{L_{Chopper}} \cdot \int_0^{Ton} V_{BAT}\, dt \tag{6}$$

$$V_{BAT} + V_{LChopper} = V_{Cbus} \tag{7}$$

$$I_L = \frac{1}{L_{Chopper}} \cdot \int_{Ton}^{Toff} (V_{BAT} - V_{Cbus})\, dt \tag{8}$$

Handling the ratio relation between the chopper sides is possible through a Pulse Width Modulation (PWM) signal, where the drive (T_{on}) and cut-off (T_{off}) times form one switching period (T) for each power switch. The voltage conversion ratio of this circuit is given by the duty-cycle (D), which can be defined by (9) and (10) for the buck mode, and by (11) and (12) for the boost mode [26].

$$D = \frac{T_{on}}{T} \tag{9}$$

$$V_{BAT} = V_{Cbus} \cdot \frac{T_{on}}{T} = V_{Cbus} \cdot D \tag{10}$$

$$\frac{1}{1 - D} = \frac{V_{Cbus}}{V_{BAT}} \Leftrightarrow D = -\frac{V_{BAT}}{V_{Cbus}} + 1 \tag{11}$$

$$V_{BAT} = V_{Cbus} \cdot (1 - D) \tag{12}$$

The inductor ($L_{Chopper}$) and the DC bus capacitor ($Cbus$) are determinant elements in the operation of this converter. The inductor works as an energy gauge to determine the energy to be released for each chopper side (in buck or boost mode), having also a role in controlling the source current ripple and mitigating some higher switching frequency effects [26]. This inductor should be sized considering the higher power level when the battery voltage is lower, independently of the operation mode. For the buck mode, equation (13) results:

$$L_{Chopper} = \frac{V_{Cbus} - V_{BAT_{nom}}}{2 \cdot \Delta I_L} \cdot T_{on} \tag{13}$$

Using (9) and (10), (14) is obtained:

$$DT = T_{on} \rightarrow \begin{cases} T_{on\_\min} = \frac{V_{BAT_{\min}}}{V_{Cbus}} \cdot T \\ T_{on\_\max} = \frac{V_{BAT_{\max}}}{V_{Cbus}} \cdot T \end{cases} \tag{14}$$

where $V_{Cbus} = 325$ V, $V_{BAT_{\min}} = 75$ V, $V_{BAT_{\max}} = 127.5$ V, and $T = 50\ \mu$s. Therefore, the values for $T_{on\_\min}$ and $T_{on\_\max}$ are 12 and 20 μs, respectively ($D = 0.24$ and $D = 0.4$).

Considering a 1.2 A current ripple (ΔI_L) criterion and the higher T_{on} value (20 μs) over (13) and $V_{BATnom} = 96V$, then $L_{Chopper}$ comes 1.9 mH.

For the boost mode analysis, (15) was used:

$$\Delta I_L = \frac{V_{BAT}}{2 \cdot L} \cdot DT \Leftrightarrow \Delta I_L = \frac{V_{BAT}}{2 \cdot L} \cdot T_{on} \tag{15}$$

Using (9) and (11), equation (16) results:

$$DT = T_{on} \rightarrow \begin{cases} T_{on\_\min} = 1 - \frac{V_{BAT_{\max}}}{V_{Cbus}} \cdot T \\ T_{on\_\max} = 1 - \frac{V_{BAT_{\min}}}{V_{Cbus}} \cdot T \end{cases} \tag{16}$$

where the values for V_{Cbus}, $V_{BAT_{\min}}$, $V_{BAT_{\max}}$, T, ΔI_L and $V_{BAT_{nom}}$ are the same used before. Using the highest T_{on} value for the buck case (38 μs) then $L_{Chopper} = 1.52$ mH. Therefore, in a way

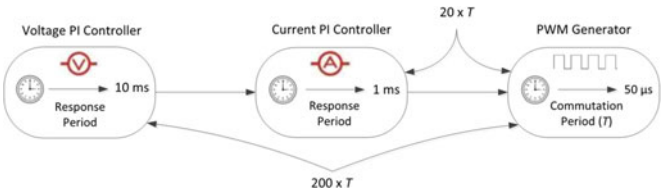

Fig. 2. DC/DC converter controller time structure.

to behold the worst-case scenario, a 1.9 mH chopper inductor was used.

The DC_{bus} capacitor is essentially used for assisting the stabilization of DC_{bus} voltage with low ripple. The $Cbus$ sizing was made taking into account the need for a stable DC_{bus} voltage during the $L_{Chopper}$ current regulation. In fact, these capacitors need to support the DC_{bus} energy demand for a higher time than the highest $L_{Chopper}$ current regulation time (38 μs), because the controllers cannot attain the desired reference in one single switching period ($T = 50$ μs) due to the load demand. Therefore, considering (17) and (18), the maximum DC_{bus} current ($I_{\max}$) is 7.07 A.

$$I_{DCbus\_\max} = \frac{P_{\max}}{V_{Cbus}} \tag{17}$$

with a 8.13 V DC_{bus} voltage ripple ($\Delta_{V_{Cbus}}$) and $\Delta t = 38$ μs. $Cbus = 33$ μF is required for one single T using (18) [26].

$$Cbus = I_{\max} \frac{\Delta t}{\Delta_{V_{Cbus}}} \tag{18}$$

Given the chopper controller time structure described in Fig. 2, the final $Cbus$ value needs to be 200 times higher than the one determined by (18), and therefore a 10mF $Cbus$ capacitor was used.

C. AC/DC Converter Circuit Analysis

In order to achieve the desirable characteristics of the charger, an AC/DC converter was also used (Fig. 1) working as a controlled rectifier and an inverter for G2V and V2G operation modes, respectively. Thus, for each operation mode, it is possible controlling the power switch drive allowing AC or DC voltage flexibility, lower voltage ripple and higher efficiency (given the lower internal IGBT resistance and the unipolar PWM generation method).

Applying the unipolar switching method, and in order to satisfy Kirchoff voltage law, the switches on the same leg (see Fig. 1) are not turned on at the same time, which gives the condition $S_1 + S_2 = 1$ for the first leg and the same is applied to the two other legs. This enables the output voltage to fluctuate between $\frac{V_{Cbus}}{2}$ and $-\frac{V_{Cbus}}{2}$ (see Fig. 1).

The voltages V_{an} and V_{bn} are the output voltages from phases a and b to an arbitrary point n. V_{no} is the neutral voltage between point n and the mid-point of the DC bus. The switching function of the devices can be approximated by the Fourier series to be equal to $\frac{1}{2} \cdot (1 + m_i)$ where m_i is the modulation signal, which yields the switching pulses when compared with the carrier (triangular waveform). Using a unipolar switching scheme, each IGBT is turned "on" and "off" based on the comparison of the carrier signal with the modulation signal (sinusoid) and its symmetric. The results of this comparison are presented in Table I.

TABLE I
UNIPOLAR INVERTER RULES

S_1	S_2	S_3	S_4	V_{an}	V_{bn}	$V_{ab} = V_{an} - V_{bn}$
on	–	–	on	V_{Cbus}	0	V_{Cbus}
–	on	on	–	0	V_{Cbus}	-V_{Cbus}
on	–	on	–	V_{Cbus}	V_{C_bus}	0
–	on	–	on	0	0	0

The fundamental component of the output voltage is given by (19):

$$\begin{cases} V_{ab} = m_i \cdot V_{Cbus} \text{ if } m_i \leq 1 \\ V_{Cbus} < V_{ab} < \frac{\pi}{4} \cdot V_{Cbus} \text{ if } m_i > 1 \end{cases} \tag{19}$$

For the controlled rectifier the same principle is used, being the PI controllers responsible for the DC_{bus} voltage and AC current control.

Based on Fig. 1, an inductive filter on the AC side of the converter was used to improve the power factor, increase PQ and mitigate some possible current spikes, which is a typical low-cost solution. This inductor size is 7.6 mH following the expression presented in (20) [27], [28].

$$L_{AC} = \frac{2 \cdot \left(V_{RMS_{AC}}\right)^2 \left(5.2 \times 10^{-2}\right)}{\omega P} \tag{20}$$

where $V_{RMS_{AC}} = 230$ V, $\omega = 2\pi f_{grid}$ and $P = 2.3$ kW.

III. CONTROLLERS DESIGN

The controllers are PI-based and they aim at properly controlling the IGBT switching following voltage and current references.

A. Chopper Controller

For the chopper controller design, some assumptions were made to facilitate circuit analysis: capacities in both sides of the chopper are high enough for considering constant voltage, low L capacity (when compared to the $Cbus$ capacity), and negligible switching losses.

For establishing the control laws, it was necessary to determine the differential equations describing the energy demand of the converter (see (21)–(24)), according to Kirchhoff laws. Typically, the state variables in the converters are associated with the energy stored in capacitors and inductors, leading to V_{Cbus} in the DC bus, V_{BAT} in the batteries, and I_L in the chopper inductor as displayed in Fig. 1.

When S_5 and S_6 are in the "on" and "off" state, respectively, $I'_L = I_L$ as a result of (21) and (22).

$$I = -I_C + I'_L \Leftrightarrow C_{bus} \cdot \frac{dV_{Cbus}(t)}{dt} = -I(t) + I_L(t) \tag{21}$$

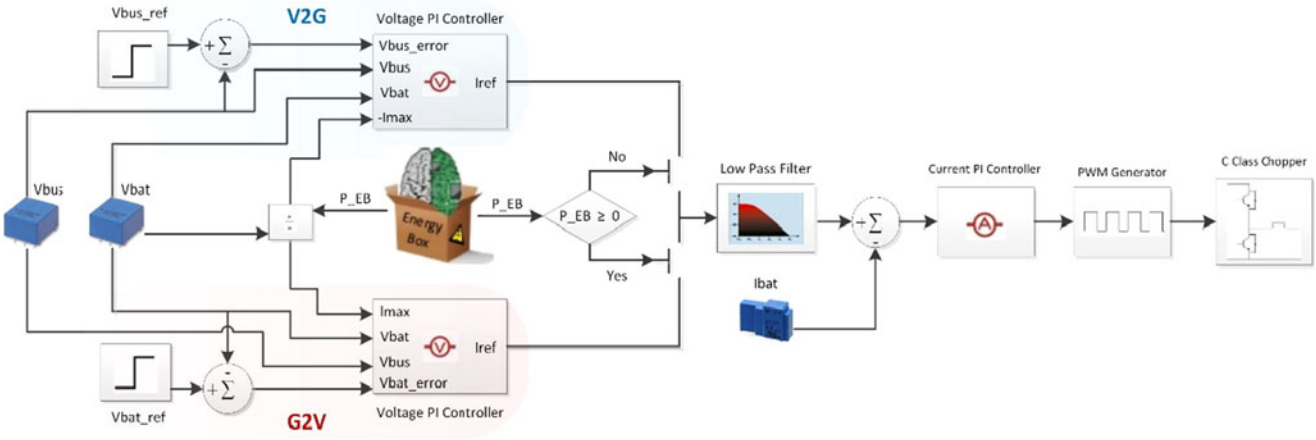

Fig. 3. DC/DC converter controller architecture for V2G and G2V operation modes, respectively.

$$V_L + V_{BAT} - V_{Cbus} = 0 \Leftrightarrow L_{Chopper} \cdot \frac{di(t)}{dt} = -V_{BAT}(t) + V_{Cbus}(t) \quad (22)$$

The second operation occurs when S_5 and S_6 are at states "off" and "on", respectively, where $I'_L = 0$ and $I_L \neq 0$ as a result of (23) and (24).

$$I = I_C + I'_L \Leftrightarrow I = Cbus \cdot \frac{dv(t)}{dt} \quad (23)$$

$$V_L + V_{BAT} = 0 \Leftrightarrow L_{Chopper} \cdot \frac{dI_L(t)}{dt} = -V_{BAT}(t) \quad (24)$$

The chopper controllers for V2G and G2V are based on two PI daisy chain architectures (see Fig. 3), which are capable to perform an effective power level control for each operation mode. This power level control is made firstly by stabilizing the DC bus and the batteries voltage for V2G and G2V, respectively. These voltage references are well-defined values, as presented in Table II.

Then, the ratio between the available power signal from the EMS (considering the loads already in operation) and the measured battery voltage imposes the current limit output response of the voltage controller. Thus, this controller dynamically restricts the current reference, based on the available power signal from the EMS. The current controller needs to be tuned in order to control I_L, being important to ensure a response time at least 20 times faster than the switching period, and with a dynamics 10 times higher than the voltage controller as presented in Fig. 2 [26], [29]. Given the previously mentioned $Cbus$ sizing methodology, it is possible to consider that V_{Cbus} is constant along the regulation of I_L. Thus, applying the Laplace transform, (22) is transformed into (25).

$$I_L = -\frac{V_{BAT}}{L_{Chopper}s} + (1 - d(s))\frac{V_{Cbus}}{L_{Chopper}s} \quad (25)$$

In order to obtain the closed loop transfer function, it is possible to define our system according to (26); then knowing the PI controller transfer function presented in (27), the close loop transfer function presented in (28) is obtained.

TABLE II
GLOBAL SYSTEM SPECIFICATIONS

Energy Levels	
$V_{AC_{RMS}}$	230 V
$I_{AC\_Max_{RMS}}$	10 A
P_{Max}	2.3 kW
$V_{DC_{Bus}}$	325 V
$V_{Bat_{\text{Max}}}$	127.5 V
$I_{Bat_{\text{Max}}}$	30 A
Passive Elements Size	
L_{AC}	7.6 mH
C_{Bus}	10 mF
$L_{chopper}$	1.9 mH
PI Controllers Values	
fs	20 kHz
PI Current Chopper's Controller: $K_P = 0.0522$; $K_I = 163.98$; $W_n = 6283.19$ rad.s^{-1}; $\tau = 3.10e^{-4}$ s	
PI Voltage Chopper's Controller: $K_P = 12.56$; $K_I = 3.97$; $W_n = 628.319$ rad.s^{-1}; $\tau = 0.0032$ s	
PI Current Rectifier's Controller: $K_P = 5.2$; $K_I = 1.3$	
PI Voltage Rectifier's Controller: $K_P = 11.7$; $K_I = 0.87$	

$$P(s) = \frac{V_{Cbus}}{L_{Chopper}s} \quad (26)$$

$$C(s) = K_P + \frac{K_I}{s} \quad (27)$$

$$G_{cl}(s) = \frac{C(s)P(s)}{1+C(s)P(s)} = \frac{\frac{V_{Cbus}}{L_{Chopper}s}\left(K_P + \frac{K_I}{s}\right)}{1+\frac{V_{Cbus}}{L_{Chopper}s}\left(K_P + \frac{K_I}{s}\right)} \quad (28)$$

The transfer function presented in (28) can be rewritten as (29), accordingly to [29], where τ is given by the K_P/K_I ratio, ξ is the damping ratio and W_n is the undamped natural frequency.

$$G_{cl}(s) = \frac{W_n^2}{s^2 + 2\xi W_n s + W_n^2} \quad (29)$$

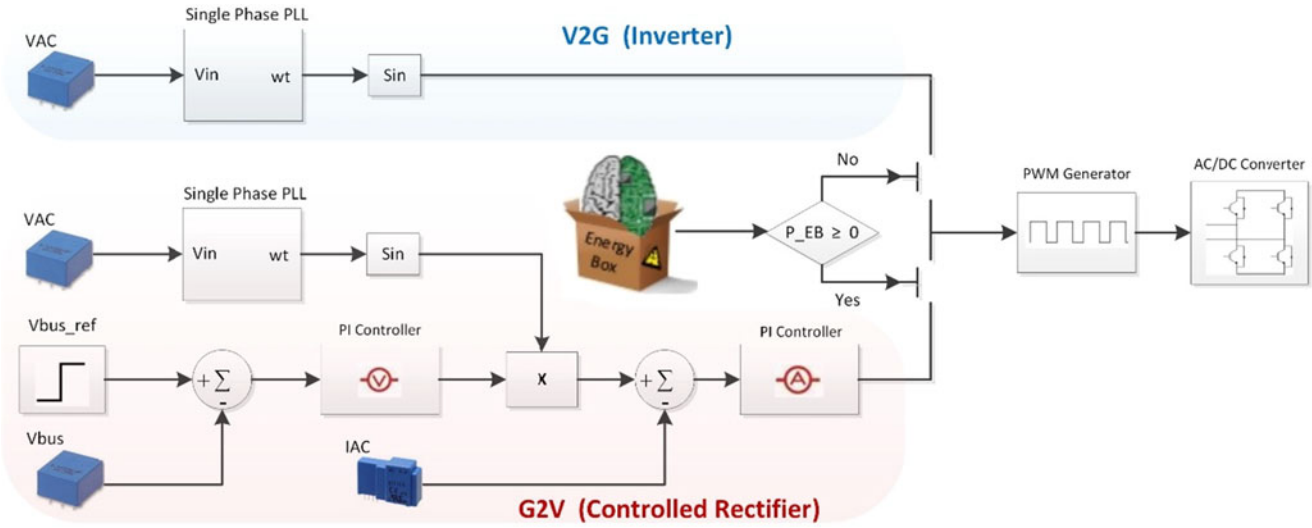

Fig. 4. AC/DC converter controller architecture for V2G and G2V operation modes.

Defining the desired second order dynamics and adding a third non-dominant pole, equation (30) results:

$$s^3 + (a_1 + b_0 K_D)\, s^2 + (a_0 + b_0 K_P)\, s + b_0\, K_I = 0 \quad (30)$$

from which the K_P (31) and K_I (32) gains can be computed. By analogy with [29], $b_0 = V_{bus}$ and $p = L$.

$$K_P = \frac{2p\xi W_n}{b_0} \Leftrightarrow \xi = \frac{K_P\sqrt{\frac{b_0}{p}}}{2\sqrt{K_I}} \quad (31)$$

$$K_I = \frac{P{W_n}^2}{b_0} \Leftrightarrow W_n = \sqrt{\frac{b_0}{p}K_I} \quad (32)$$

In order to perform the power control and ensure DC_{bus} and battery voltage disturbance rejection, a second PI controller is designed for the voltage according to the same principle previously specified for the current. This PI daisy chain operates correctly considering a voltage loop 10 times slower than the current loop, as well as no chopper losses and $L_{Chopper}$ capacity much lower than the $Cbus$ capacity. Thus, a relation can be obtained through the average model, as presented in (33).

$$V_{BAT}\, I_L = V_{Cbus}\, {I'}_L \Leftrightarrow \frac{V_{BAT}}{V_{Cbus}} = \frac{{I'}_L}{I_L} \quad (33)$$

Using (33), (21) can be rewritten as presented in (34) after the application of Laplace transform.

$$I = -I_C + I'_L \Leftrightarrow {I'}_L = I + sCbus V_{Cbus} \quad (34)$$

Therefore combining (33) and (34), (35) is obtained.

$${I'}_L = I + sCbus\frac{I_L}{{I'}_L}V_{BAT} \quad (35)$$

Being V_{Cbus} and V_{BAT} measurable variables, it is possible deciding whether DC_{bus} or the battery voltage is controlled through (35), leading to (36) and (37) for V2G and G2V operation modes, respectively. Therefore, two different voltage PI chopper controllers are obtained, as presented in Fig. 3.

$$V_{Cbus}(s) = \frac{1}{sCbus}\left({I'}_L - I\right) \quad (36)$$

$$V_{BAT}(s) = \frac{V_{BAT}}{V_{Cbus}}\frac{1}{sCbus}\left({I'}_L - I\right) \quad (37)$$

Thus, using a similar approach as the one used for the current, the voltage controller is tuned through (38) and (39), where $\frac{1}{sCbus}$ was the plant model considered. For both PI controllers $\xi = 1$ was considered avoiding the transient response overshoot.

$$K_I = {W_n}^2 C_{bus} \Leftrightarrow W_n = \sqrt{\frac{K_I}{C_{bus}}} \quad (38)$$

$$\frac{1}{K_p} = \frac{\sqrt{\frac{1}{Cbus}}}{2\xi\sqrt{K_I}} \Leftrightarrow \xi = \frac{K_P\sqrt{\frac{1}{Cbus}}}{2\sqrt{K_I}} = \frac{K_P}{2\sqrt{Cbus\cdot K_I}} \quad (39)$$

B. AC/DC Converter Controller

The controller for the rectifier is also PI based. A daisy chain of two PI controllers for DC_{bus} voltage and AC current regulation is used. For AC current regulation, a phase-locked loop (PLL) is also used providing AC current control reference as stated in [30]. This controller was firstly tuned using a pole placement approach and then refined through experimental tests, being the final IGBT PWM signal provided by the unipolar PWM generator.

The controller used for the AC/DC converter when this works as inverter is based only on the unipolar switching method. A unit sinusoid reference provided by a PLL is used, which is synchronized with the voltage grid. In this operation mode, the DC_{bus} available power was already restricted by the chopper, being at this point only mandatory inverting the DC_{bus} voltage in a proper way. Both AC/DC converter controllers are presented in Fig. 4

Data for the proposed charger topology and the designed controllers are summarized in Table II.

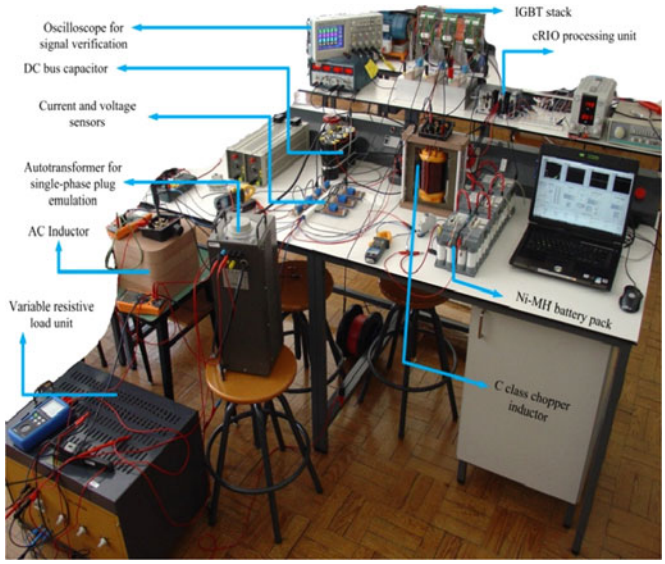

Fig. 5. Reduced-scale experimental setup for the proposed charger validation.

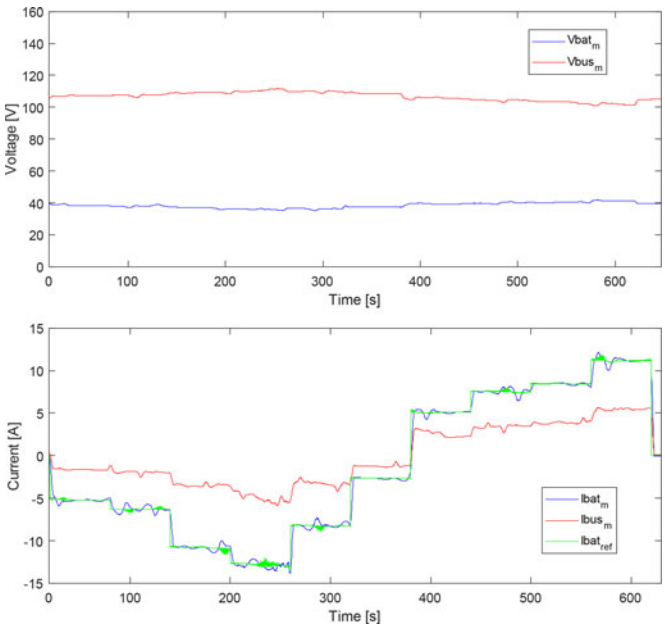

Fig. 6. Voltage and current values obtained in the chopper for the full profile.

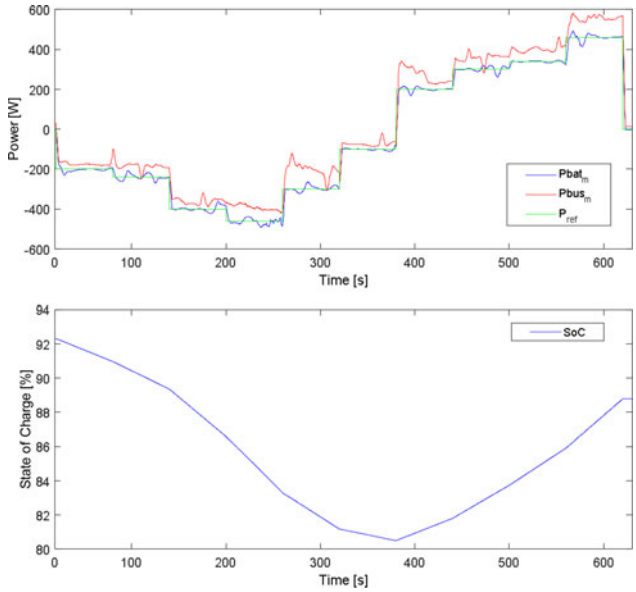

Fig. 7. Full charger power profile and corresponding battery SoC evolution.

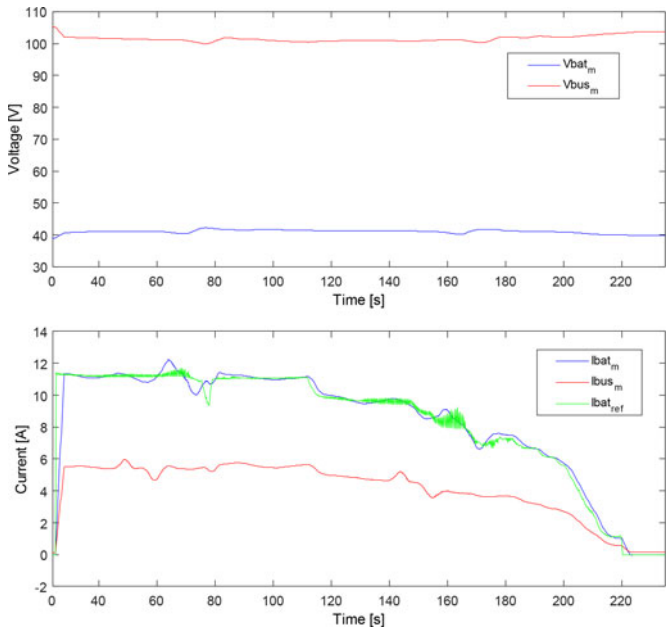

Fig. 8. Absorbed battery current evolution up to 100% of SoC.

IV. Experimental Results

The experimental results have been obtained using a reduced scale setup (with power levels 5 times lower than the full scale). It is important to note that in this reduced scale setup the DC_{BUS} voltage was stabilized around 108 V and P_{Max} was $\pm$460 W, being the "Advisable Energy Levels" presented in Table II used for sizing, simulation and further full-scale implementation. This setup uses the LEM HY25-P and LV 25-P transducers for current and voltage acquisition, respectively, as presented in Figs. 3 and 4. A DSP from NI for control and data logging purpose is also used, jointly with other laboratory equipment and several electronic components, as presented in Fig. 5

The experimental results obtained for voltage, current and power at the batteries and DC_{bus} are presented in Figs. 6 and Fig. 7, including the batteries SoC (State-of-Charge). In Figs. 6 and 7 the dynamic current adjustment is verified under each power reference, where the voltages are stable around the expectable values, in particular for the DC_{bus}.

The battery voltage does not suffer significant changes due to the use of two Ni-MH parallel battery pack of 36 V nominal voltage each. This battery pack presents a very good capacity, not being subject to the peak power for more than one minute. The methodology proposed can also be used with other battery chemistries.

The sequence of P_{ref} levels was designed to verify the charger's dynamic behavior with a sequence of different power steps respecting the power restrictions of the reduced scale setup. Figs. 8 and 9 present a 0.5 second transient response from 0 to

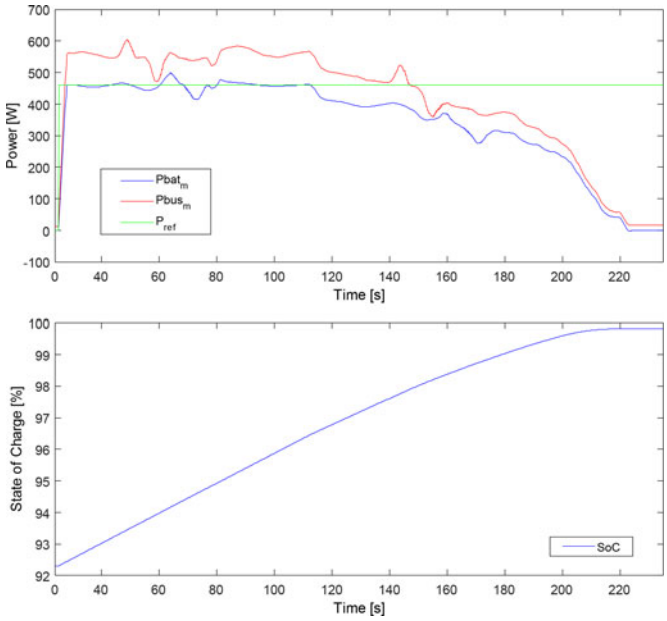

Fig. 9. Charging power profile and corresponding battery SoC evolution for 460 W.

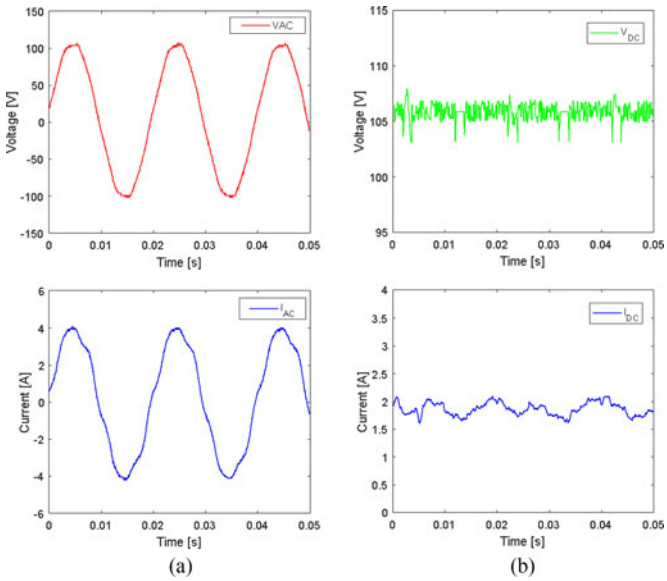

Fig. 10. Controlled rectifier voltage and current curves for 200 W in (a) AC side and (b) DC_{bus} side.

460 W. Even with the control and acquisition routines not implemented in the FPGA but only in the real-time processor, which has a higher response time, the system can rise from 0 to P_{Max} in 0.5 s. Figs. 10 and 11 present the AC and DC_{BUS} voltage and current curves for G2V (controlled rectifier) and V2G (inverter) operation modes, respectively. It is possible to verify the adequate operation of both modes for two random power levels, i.e., 200 W and 240 W, respectively.

The power values obtained verify the correct establishment of their set points for G2V and V2G operation modes. The SoC also presents a narrow evolution in both modes due to the

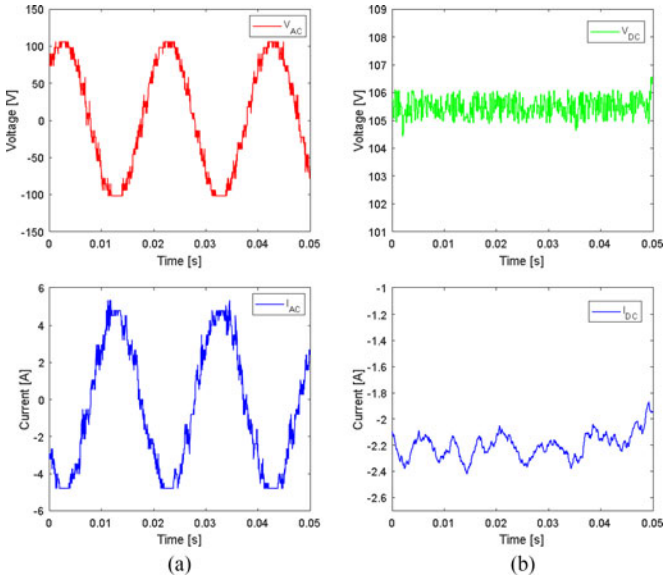

Fig. 11. Inverter voltage and current curves for 240 W in (a) AC side and (b) DC_{bus} side.

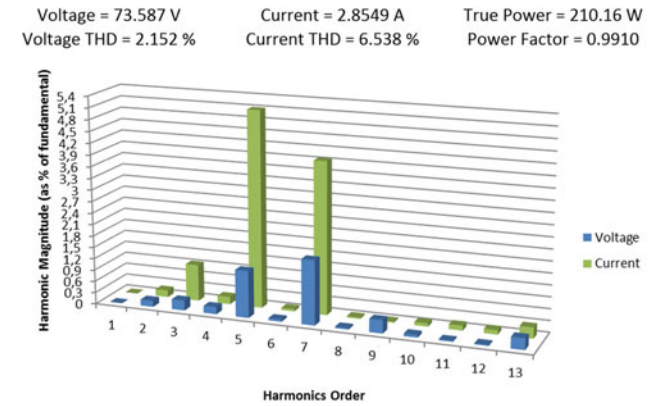

Fig. 12. AC/DC converter THD analysis for a controlled rectifier (G2V mode).

small-time slot of the power pattern applied and the previously mentioned characteristics of the Ni-MH parallel battery pack.

Fig. 8 presents the current and Fig. 9 the power and SoC for the case where the batteries SoC approaches 100%, for 460 W power level, displaying the setting of the correct power reference and the corresponding decreasing charging current value according to SoC evolution. When the SoC quickly reaches 100%, the local battery controller adjusts the charge to the actual level of the energy stored in the battery to prevent battery damages. As displayed in Figs. 8 and 9, the power applied to the battery is progressively reduced as a function of its SoC.

Figs. 12 and 13 enable to verify that for each case previously presented in Figs. 10 and 11, the power factor achieved is practically one and a low THD results. Thus, this charger presents a low PQ impact on the interconnection point, which lies within the international standards (voltage THD $< 5\%$ and current THD $< 8\%$) [22].

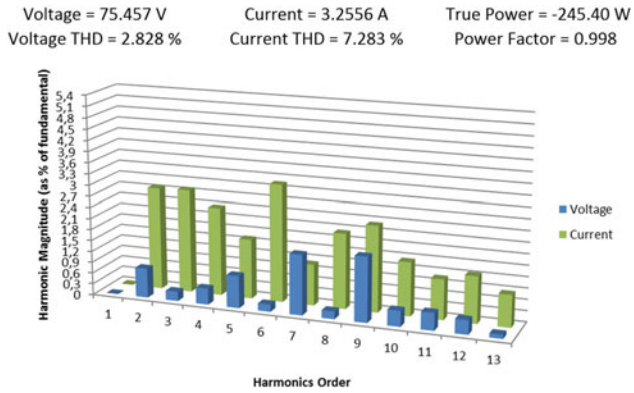

Fig. 13. AC/DC converter THD analysis for inverter (V2G mode).

V. Conclusion

This paper proposes a simple and functional bidirectional PEV (or stationary battery) charger topology, which allows enhancing the capabilities of a joint operation of storage and an autonomous EMS in a residential setting, with potential benefits for end-users and utilities/system operator. The PEV role as load or power supplier is also emphasized. This charger is adjustable for charging or discharging operations using a power level provided by the EMS, instead of minimizing the charging time by using only the maximum power level. Since the charger is power flexible and bidirectional, its power electronics topology allows performing charge/discharge operations at different power levels, which benefits the integrated power allocation and scheduling among all residential loads. The end-user just needs to indicate the instant he/she needs the vehicle and the EMS determines the optimal charging (and possible selling energy back to the grid) according to that requirement and the information from other loads and price signals from the grid.

The validation of the proposed charger has been performed using a reduced scale experimental setup based on DSP technology. The illustrative results presented foresee an adequate interaction between the charger and an autonomous EMS, in which the stipulated power limits are fulfilled and the PQ impact on the interconnection point lies within the international standards for both operation modes (G2V and V2G). This methodology can be used also for higher power (single-phase) and is compatible with any battery chemistry and its particular voltage, current and depth of discharge limits.

References

[1] D. Livengood and R. Larson, "The energy box: Locally automated optimal control of residential electricity usage," *Serv. Sci.*, vol. 1, no. 1, pp. 1–16, 2009.

[2] A. Soares, Á. Gomes, C. H. Antunes, and C. Oliveira, "A customized evolutionary algorithm for multiobjective management of residential energy resources," *IEEE Trans. Ind. Informat.*, vol. 13, no. 2, pp. 492–501, Apr. 2017.

[3] M. Lopes *et al.*, "An automated energy management system in a smart grid context," in *Proc. IEEE Int. Symp. Sustain. Syst. Technol.*, 2012, p. 1.

[4] A. Soares, H. Melo, C. H. Antunes, J. P. Trovao, A. Gomes, and H. Jorge, "Integration of the electric vehicle as a manageable load in a residential energy management system," in *Proc. IEEE Veh. Power Propulsion Conf.*, Montreal, QC, Canada, 2015, pp. 1–6.

[5] H. N. Melo, J. P. Trovão, P. G. Pereirinha, and H. Jorge, "Electric vehicles' intelligent charger for automated energy management system," in *Proc. Int. Workshop Energy Efficiency More Sustain. World*, Azores, Portugal, 2012, pp. 1–6.

[6] H. N. Melo, J. P. Trovão, C. H. Antunes, P. G. Pereirinha, and H. Jorge, "An outlook of electric vehicle daily use in the framework of an energy management system," *Manag. Environ. Qual.: Int. J.*, vol. 26, no. 4, pp. 588–606, 2015.

[7] H. N. Melo, J. P. Trovão, P. G. Pereirinha, and H. Jorge, "Energy profits with controllable electric vehicle's charger under energy box decisions," in *Proc. 7th Int. Conf. Energy Efficiency Domestic Appliances Lighting*, Coimbra, Portugal, 2013, pp. 1–6.

[8] V. Monteiro, J. P. Carmo, J. G. Pinto, and J. L. Afonso, "A flexible infrastructure for dynamic power control of electric vehicle battery chargers," *IEEE Trans. Veh. Technol.*, vol. 65, no. 6, pp. 4535–4547, Jun. 2016.

[9] I. Vittorias, M. Metzger, D. Kunz, M. Gerlich, and G. Bachmaier, "A bidirectional battery charger for electric vehicles with V2G and V2H capability and active and reactive power control," in *Proc. IEEE Transp. Electrific. Conf. Expo*, Dearborn, MI, USA, 2014, pp. 1–6.

[10] M. I. Milanés-Montero, M. A. G. Martínez, E. González-Romera, E. Romero-Cadaval, and F. Barrero-González, "Active and reactive power control strategies for electric vehicles in smart grids," in *Proc. 10th Int. Conf. Compat., Power Electron. Power Eng.*, Bydgoszcz, Poland, 2016, pp. 114–119.

[11] N. Tashakor, E. Farjah, and T. Ghanbari, "A bidirectional battery charger with modular integrated charge equalization circuit," *IEEE Trans. Power Electron.*, vol. 32, no. 3, pp. 2133–2145, Mar. 2017.

[12] R. Zgheib, K. Al-Haddad, and I. Kamwa, "V2G, G2V and active filter operation of a bidirectional battery charger for electric vehicles," in *Proc. IEEE Int. Conf. Ind. Technol.*, Taipei, Taiwan, 2016, pp. 1260–1265.

[13] J. G. Pinto, V. Monteiro, H. Gonçalves, and J. L. Afonso, "Onboard reconfigurable battery charger for electric vehicles with traction-to-auxiliary mode," *IEEE Trans. Veh. Technol.*, vol. 63, no. 3, pp. 1104–1116, Mar. 2014.

[14] V. Monteiro, J. G. Pinto, and J. L. Afonso, "Operation modes for the electric vehicle in smart grids and smart homes: Present and proposed modes," *IEEE Trans. Veh. Technol.*, vol. 65, no. 3, pp. 1007–1020, Mar. 2016.

[15] L. Solero, "Nonconventional on-board charger for electric vehicle propulsion batteries," *IEEE Trans. Veh. Technol.*, vol. 50, no. 1, pp. 144–149, Jan. 2001.

[16] B. Bilgin, A. Emadi, and M. Krishnamurthy, "Design considerations for a universal input battery charger circuit for PHEV applications," in *Proc. IEEE Int. Symp. Ind. Electron.*, 2010, pp. 3407–3412.

[17] O. C. Onar, J. Kobayashi, D. C. Erb, and A. Khaligh, "A bidirectional high-power-quality grid interface with a novel bidirectional noninverted buck–boost converter for PHEVs," *IEEE Trans. Veh. Technol.*, vol. 61, no. 5, pp. 2018–2032, Jun. 2012.

[18] Y. J. Lee, A. Khaligh, and A. Emadi, "Advanced integrated bidirectional AC/DC and DC/DC converter for plug-in hybrid electric vehicles," *IEEE Trans. Veh. Technol.*, vol. 58, no. 8, pp. 3970–3980, Oct. 2009.

[19] S. Haghbin, S. Lundmark, M. Alakula, and O. Carlson, "An isolated high-power integrated charger in electrified-vehicle applications," *IEEE Trans. Veh. Technol.*, vol. 60, no. 9, pp. 4115–4126, Nov. 2011.

[20] R. Baharom, M. K. M. Salleh, M. N. Seroji, and M. K. Hamzah, "A high power factor bidirectional battery charger using single-phase matrix converter," in *Proc. IEEE 10th Conf. Ind. Electron. Appl.*, Auckland, New Zealand, 2015, pp. 1397–1402.

[21] F. Marra, M. M. Jensen, R. Garcia-Valle, C. Traholt, and E. Larsen, "Power quality issues into a Danish low-voltage grid with electric vehicles," in *Proc. 11th Int. Conf. Elect. Power Qual. Utilisation*, 2011, pp. 1–6.

[22] J. P. Trovão, P. G. Pereirinha, L. Trovao, and H. Jorge, "Electric vehicles chargers' characterization: Load demand and harmonic distortion," in *Proc. 11th Int. Conf. Elect. Power Qual. Utilisation*, 2011, pp. 1–7.

[23] C. C. Chan, Y. S. Wong, A. Bouscayrol, and K. Chen, "Powering sustainable mobility: Roadmaps of electric, hybrid and fuel cell vehicles," *Proc. IEEE*, vol. 97, no. 4, pp. 603–607, Apr. 2009.

[24] O Hegazy, J. Van Mierlo, and J. Lataire, "Design and control of bidirectional DC/AC and DC/DC converters for plug-in hybrid electric vehicles," in *Proc. Int. Conf. Power Eng., Energy Elect. Drives*, 2011, pp. 1–7.

[25] J. P. F. Trovão, M. A. Roux, É. Ménard, and M. R. Dubois, "Energy- and power-split management of dual energy storage system for a three-wheel electric vehicle," *IEEE Trans. Veh. Technol.*, vol. 66, no. 7, pp. 5540–5550, Jul. 2017.

[26] M. A. Silva, J. P. Trovão, and P. G. Pereirinha, "Implementation of a multiple input DC-DC converter for Electric Vehicle power system," in *Proc. 3rd Int. Youth Conf. Energetics*, 2011, pp. 1–8.

[27] S. B. Dewan, "Optimum input and output filters for a single-phase rectifier power supply," *IEEE Trans. Ind. Appl.*, vol. IA-17, no. 3, pp. 282–288, May 1981.
[28] M. Borage, S. Tiwari, and S. Kotaiah, "Passive techniques for compliance of single-phase rectifiers with IEC 1000-3-2 norms," in *Proc. 8th Int. Conf. Electromagn. Interference Compat.*, 2003, pp. 1–8.
[29] T. Azib, O. Bethoux, G. Remy, C. Marchand, and E. Berthelot, "An innovative control strategy of a single converter for hybrid fuel cell/supercapacitor power source," *IEEE Trans. Ind. Electron.*, vol. 57, no. 12, pp. 4024–4031, Dec. 2010.
[30] A. Kumar and R. Gupta, "Single-phase AC/DC/AC converter using cascaded multilevel inverter," in *Proc. Int. Conf. Power, Control Embedded Syst.*, 2010, pp. 1–5.

Hugo Neves de Melo received the M.Sc. degree in electrical engineering (automation) from the University of Coimbra, Coimbra, Portugal, in 2012. From 2012 to 2015, he was a Full-Time Researcher with the Institute for Systems Engineering and Computers at Coimbra, Coimbra. Since 2015, he has been an Architect and Systems Engineer with the Distribution System Operator, Energias de Portugal, Lisbon, Portugal. His research interests include energy management, electric vehicles, smart grids, control systems, electronics, and battery technology.

João Pedro F. Trovão (S'08–M'13–SM'17) received the Ph.D. degree in electrical engineering (power systems) from the University of Coimbra, Coimbra, Portugal, in 2013. He is currently a Professor with the Department of Electrical Engineering and Computer Engineering, University of Sherbrooke, Sherbrooke, QC, Canada, where he holds the Canadian Research Chair position in Efficient Electric Vehicles with Hybridized Energy Storage Systems.

Dr. Trovão was the General co-Chair and the Technical Program Committee (TPC) co-Chair of the 2014 IEEE Vehicle Power and Propulsion Conference (VPPC). He is the TPC co-Chair of the 2017 IEEE VPPC. He is a founding member and the co-Director of the electric-Transport, Energy Storage and Conversion Laboratory of the University of Sherbrooke.

Paulo G. Pereirinha (S'04–M'06–SM'17) received the Ph.D. degree in electrical engineering from the University of Coimbra, Coimbra, Portugal, in 2005. He is a Coordinator Professor with the Coimbra Institute of Engineering, Polytechnic Institute of Coimbra, Coimbra. His research interests include electrical machines, electric vehicles, and electromechanical drives. He was the General Chair of the 2014 IEEE Vehicle Power and Propulsion Conference (VPPC), the Publication Chair of 2015 IEEE VPPC, and the Award-Committee Chair of the 2016 IEEE VPPC. He is a member of the Vehicular Power Propulsion Standing Advisory Committee of the IEEE Vehicular Technology Society. He is a Researcher with the Institute for Systems Engineering and Computers at Coimbra, Coimbra, and the Vice-President of the Portuguese Electric Vehicle Association.

Humberto M. Jorge (M'92) received the Ph.D. degree in electrical engineering (energy systems) from the University of Coimbra, Coimbra, Portugal, in 1999. He is an Assistant Professor with the Department of Electrical and Computer Engineering, University of Coimbra, and a Researcher with the Institute for Systems Engineering and Computers at Coimbra, Coimbra. His research interests include energy systems, energy efficiency, energy management, and demand response.

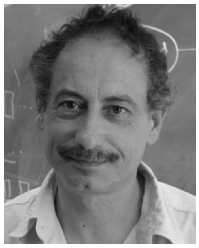

Carlos Henggeler Antunes received the Ph.D. degree in electrical engineering (optimization and systems theory) from the University of Coimbra, Coimbra, Portugal, in 1992. He is a Full Professor with the Department of Electrical and Computer Engineering, University of Coimbra, and the Director of the Institute for Systems Engineering and Computers at Coimbra, Coimbra. His research interests include multiple-objective optimization and energy planning with a focus on demand response.